CG

MET O 11 TECHNICAL NOTE NO. 158

SIMULATION OF HYDRAULIC JUMPS IN A ONE-DIMENSIONAL, ROTATING SYSTEM, USING THE RANDOM CHOICE METHOD

By

C A Parrett

Meteorological Office (Met O 11)
London Road
Bracknell
Berkshire
United Kingdom

June 1982

1. Introduction

This Technical Note describes a part of the work being undertaken in Met O 11 to look into the numerical treatment of discontinuities in the atmosphere. The development of these discontinuities (e.g. fronts) can be very complex. Here we look at a much simpler case: the formation of hydraulic jumps in a one-dimensional, rotating, homogeneous, inviscid, one-layer fluid. This process is dependent upon two non-dimensional parameters, the Rossby number, $R_o = U/fL$, and the Froude number, $F = U/(gh_m)^{\frac{1}{2}}$, where U and L are the initial velocity and length scales, h_m is the mean height of the fluid and f is the Coriolis parameter (Williams and Hori (1970), henceforward referred to as WH). Because the system rotates, there is a limiting initial scale beyond which jumps do not form, unless the time scale is greatly increased. If there were no rotation present a hydraulic jump could arise from an initial state having any horizontal scale.

This model may have direct application to various mesoscale phenomena in the atmosphere, which it is claimed are analogous to hydraulic jumps (e.g. squall lines), as well as to internal waves in the ocean (WH). All of these phenomena are affected by rotation, but the influence is not dominant as it is for large-scale motions.

Our aim was to see whether current numerical methods (i.e. finite difference (F.D.) methods) used in numerical weather prediction models correctly handle the evolution of discontinuities (in, for example, wind and potential temperature) that may form within a model or may already be present in the initial state. Here, in our simple one-dimensional model of hydraulic jumps (with discontinuities in fluid height and velocity), we have used a special one-dimensional method (the Random Choice Method (RCM)), with which to compare the F.D. methods. This method can be proved to converge to the physically relevant solution of many

systems of one-dimensional equations under certain restrictions on the data (Glimm (1965), and many later papers). It has recently been shown (Marshall and Mendez (1981), henceforward referred to as MM) that the evolution of one-dimensional jumps without rotation can be modelled numerically very well using the RCM, due to the method's ability to track discontinuities and to the fact that it does not require any artificial viscosity. Here we have adapted the method to include rotation and shown the convergence of it in this case; we have then treated the RCM solution as the correct one.

Thus, we have basically produced two numerical models based on the shallow water equations, including rotation: one utilising the RCM and the other using conventional F.D. methods. These were then used firstly to carry out a comparison run with $R_o = 0.1$ and $F = 1.0$, in which the formation of jumps was severely delayed by the high rotation rate, in order to check the RCM against the F.D. methods. For this smooth solution the F.D. model is known to converge to the correct answer. As a further check we compared them both with an identical case from WH. We then reproduced and extended some further results from WH for a case where a jump formed ($R_o = 1.0$, $F = 1.0$). They carried their integrations forward only to the point of jump formation, the criteria of which they were interested in, whereas we continued beyond its formation to compare its evolution in the two different models. Artificial diffusion was added to the F.D. model, in order to inhibit the growth of the spurious oscillations produced behind the jumps.

The two models used the shallow water equations

$$\frac{\partial u}{\partial t} + u\frac{\partial u}{\partial x} + \frac{\partial \phi}{\partial x} = fv \qquad (1),$$

$$\frac{\partial v}{\partial t} + u\frac{\partial v}{\partial x} = -fu \qquad (2),$$

$$\frac{\partial \phi}{\partial t} + \frac{\partial}{\partial x}(\phi u) = 0 \qquad (3),$$

where $\phi = gh$, h = depth of the fluid, and the three variables u, v and ϕ were independent of y.

2. The Random Choice Method

In the RCM the solution is constructed by assuming initially piecewise constant data and solving exactly for one time-step. The new field is no longer piecewise constant, and so a piecewise constant field has to be constructed from it by a sampling technique. The method evolved from Glimm's constructive existence proof (Glimm (1965)) and was developed by Chorin (1976) for solving non-linear, hyperbolic systems of conservation laws. Recently MM have used it to solve the one-dimensional shallow water equations without rotation.

The RCM is a two-step method, and in order to find $\underline{u}_{i+\frac{1}{2}}^{n+\frac{1}{2}}$ $\left[= \underline{u}\left((i+\tfrac{1}{2})\Delta x, (n+\tfrac{1}{2})\Delta t\right)\right]$ and define the method, we consider a system of conservation laws $\frac{\partial \underline{u}}{\partial t} + \frac{\partial}{\partial x}\underline{F}(\underline{u}) = 0$. At time $t_n = n\Delta t$, the method approximates the solution $\underline{u}(x, t_n)$ with piecewise constant data

$$\underline{u}(x, t_n) = \underline{u}_{i+1}^n \quad , \quad x \geqslant (i+\tfrac{1}{2})\Delta x$$
$$= \underline{u}_i^n \quad , \quad x < (i+\tfrac{1}{2})\Delta x \, ,$$

where $i\Delta x \leq x \leq (i+1)\Delta x$ (see Fig. 1). This defines a succession of Riemann problems (one for each intermediate point $(i+\tfrac{1}{2})\Delta x$), which are to be solved exactly to give the solutions $\bar{\underline{u}}(x, t_{n+\frac{1}{2}})$ at time $(n+\tfrac{1}{2})\Delta t$. These new solutions are then sampled randomly to obtain the values for the intermediate points, midway between grid-points, $(i+\tfrac{1}{2})\Delta x$. For each interval $[i\Delta x, (i+1)\Delta x]$ let θ_i be the value of a random variable θ , equidistributed in $[-\frac{1}{2}, \frac{1}{2}]$, and let P_i be the sampling point $(i+\tfrac{1}{2}+\theta_i)\Delta x$; then $\bar{\underline{u}}(P_i, t_{n+\frac{1}{2}})$ is the value of the solution of the Riemann problem at P_i . This is the value which is then ascribed to $\underline{u}$ at the point $(i+\tfrac{1}{2})\Delta x$, at time $t_{n+\frac{1}{2}} = t_n + \Delta t/2$, i.e. $\underline{u}_{i+\frac{1}{2}}^{n+\frac{1}{2}} = \bar{\underline{u}}(P_i, t_{n+\frac{1}{2}})$. Thus, we have advanced the solution forward by half a time-step to $t_{n+\frac{1}{2}}$. With a similar procedure it is then advanced from $t_{n+\frac{1}{2}}$ to t_{n+1} (the second step) to give

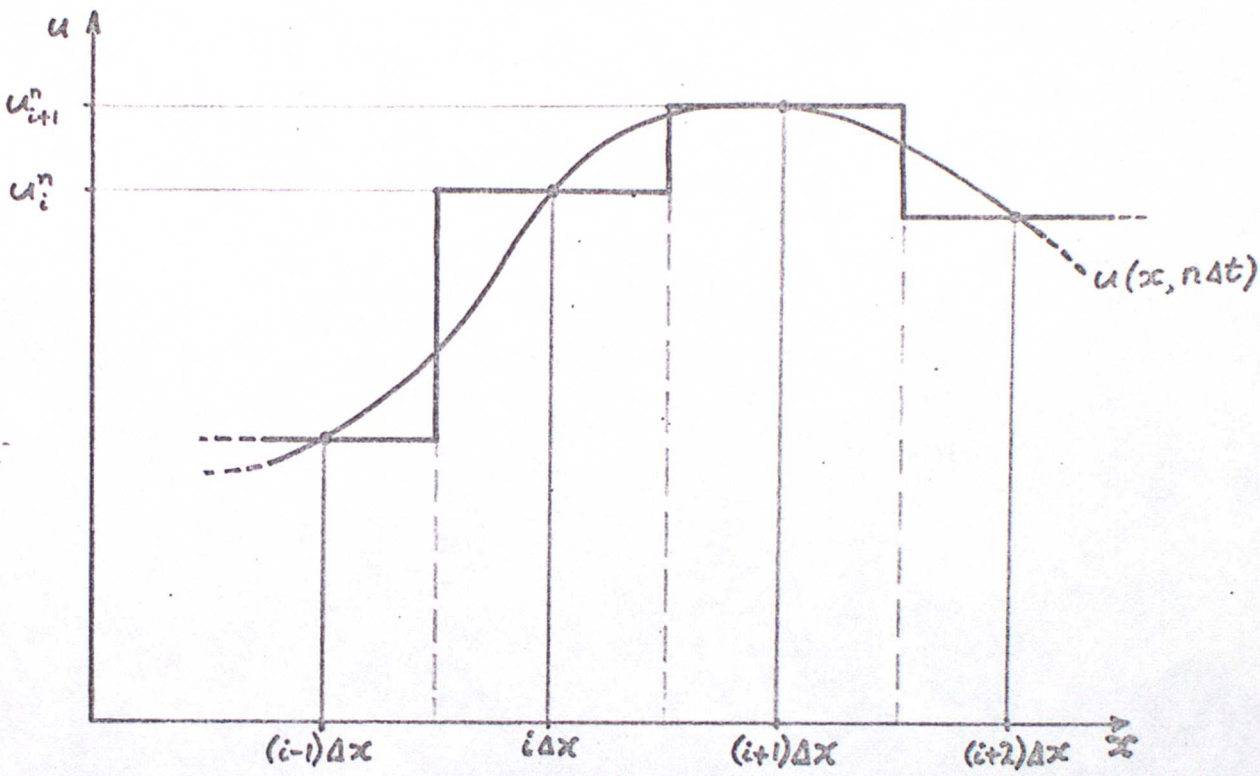

Figure 1. Approximation of $\underline{u} = (u, \ldots)$ by piecewise constant functions.

the values of u at the grid-points after one complete time-step, ready to repeat the whole process again and proceed in time.

The method depends on being able to solve the Riemann problem exactly. Chorin (1976) modified an iterative method due largely to Godunov (1959) for this purpose, in order to solve the system of equations for gas dynamics utilising the RCM. In MM they made use of the analogy between the equations of the isentropic flow of a perfect gas with constant specific heat (ie. with $\gamma = 2$) and the shallow water equations; thus enabling them to use the Chorin-Godunov iterative method to solve the Riemann problem. This they did for the case of a breaking dam, which produces a bore (or jump) travelling downstream and a depression wave moving upstream.

The system of equations solved by Marshall and Mendez was the one-dimensional shallow water system without rotation

$$\frac{\partial m}{\partial t} + \frac{\partial}{\partial x}\left(\frac{m^2}{\phi} + \phi^2\right) = 0 \qquad (4),$$

$$\frac{\partial \phi}{\partial t} + \frac{\partial m}{\partial x} = 0 \qquad (5),$$

where $m = \phi u$. To incorporate rotation into this model we include the second horizontal momentum equation and the Coriolis terms, to give the system (1), (2), (3). This system as it stands cannot be solved using the RCM, so it was solved by a splitting method, first solving

$$\frac{\partial m}{\partial t} + \frac{\partial}{\partial x}\left(\frac{m^2}{\phi} + \phi^2\right) = 0 \qquad (6),$$

$$\frac{\partial n}{\partial t} + \frac{\partial}{\partial x}\left(\frac{mn}{\phi}\right) = 0 \qquad (7) \quad (n = \phi v),$$

$$\frac{\partial \phi}{\partial t} + \frac{\partial m}{\partial x} = 0 \qquad (8),$$

which were solved using the RCM; and then adding on the Coriolis terms. Thus we were able to use the Chorin-Godunov iterative procedure (as used in MM) to solve equations (6) and (8) (which are the same as (4) and (5)) for m and ϕ, and thence solve (7) separately for n, since this equation is uncoupled from the other two.

To make use of the gas dynamic analogy (following MM), let $\rho = \rho_w h$ (9), where ρ_w is the density of water and ρ is the analogous "gas" density; and let the integrated pressure, $P = \int_h^0 p\, dz = \int_h^0 -g\rho_w z\, dz$ (using the hydrostatic assumption) $\Rightarrow P = g\rho^2/2\rho_w$ (10); i.e. the relation between pressure and density for this "γ-law gas" is $P = A\rho^\gamma$ (10a), where $A = g/2\rho_w$ and $\gamma = 2$. Then the equations (6) and (8) become

$$\partial m/\partial t + \partial/\partial x\left(\frac{m^2}{\rho} + P\right) = 0 \qquad (11)$$

$$\partial \rho/\partial t + \partial/\partial x\, m = 0 \qquad (12)$$

(where $m = \rho u$), which are identical to the equations of isentropic flow of a perfect gas with constant specific heat. In this analogy the depth of the water plays the role of the density of the gas.

System (11), (12) can be written as

$$\frac{\partial \underline{u}}{\partial t} + \frac{\partial}{\partial x}\underline{F}(\underline{u}) = 0 \qquad (13),$$

where $\underline{u} = \begin{pmatrix} m \\ \rho \end{pmatrix}$ and $\underline{F} = \begin{pmatrix} \frac{m^2}{\rho} + A\rho^2 \\ m \end{pmatrix}$, or, equivalently,

$$\frac{\partial \underline{u}}{\partial t} + B(\underline{u})\frac{\partial \underline{u}}{\partial x} = 0 \qquad (13a),$$

where $B(\underline{u}) = \begin{pmatrix} 2\frac{m}{\rho} & 2A\rho - \left(\frac{m}{\rho}\right)^2 \\ 1 & 0 \end{pmatrix}$. This enables us to obtain the slopes (dx/dt) of the two families of characteristic lines $C_\pm$, which are given by the eigenvalues of B, $\lambda_\pm = u \pm c$, where

$c = (\partial P/\partial \rho)^{1/2}$ is the sound speed. After MM the system (4), (5) can be changed to

$$\left\{ \frac{\partial}{\partial t} + (u + \bar{c}) \frac{\partial}{\partial x} \right\} J_+ = 0$$

$$\left\{ \frac{\partial}{\partial t} + (u - \bar{c}) \frac{\partial}{\partial x} \right\} J_- = 0 \quad ,$$

where $\bar{c} = (g h)^{1/2}$ (analogous to the sound speed in gas dynamics) is the speed of propagation of small disturbances relative to the fluid velocity, and $J_\pm = u \pm 2\bar{c}$. The $J_\pm$ are called Riemann Invariants and are constant along the characteristic lines $C_\pm$. When characteristics of the same family intersect a discontinuity is formed, which moves with a speed s given by the jump conditions ($s[\underline{u}] = [\underline{F}(\underline{u})]$, where $[\ldots]$ indicates the change in a quantity across the discontinuity) and the Riemann Invariants are no longer of any use. The jump conditions (and the full Rankine-Hugoniot conditions for non-isentropic flow) are obtained from the integral forms of the equations (Chorin and Marsden (1979)).

Returning to the solution of the Riemann problem, we now consider system (13), with the initial data $\underline{u}(x,0) = S_L \equiv (\rho_L, u_L)$, $x < 0$,

$= S_R \equiv (\rho_R, u_R)$, $x \geq 0$.

S_L and S_R indicate left and right initial states respectively, separated by a slip-line with $dx/dt = u_*$. The solution at later times will consist of three states : S_L , S_R and a centre state $S_* = (\rho_*, u_*)$, separated by two (centred) waves (since there are two eigenvectors for matrix $B(\underline{u})$), which may be either shocks or rarefaction waves. In our shallow water equation analogy, the shocks are replaced by hydraulic jumps and the rarefaction fans by depression waves, with the profiles of water height the same as the density profiles of Fig. 2. Figure 2 shows one of the four possible combinations of waves, with a shock wave travelling to the right (positive x-direction) and a rarefaction

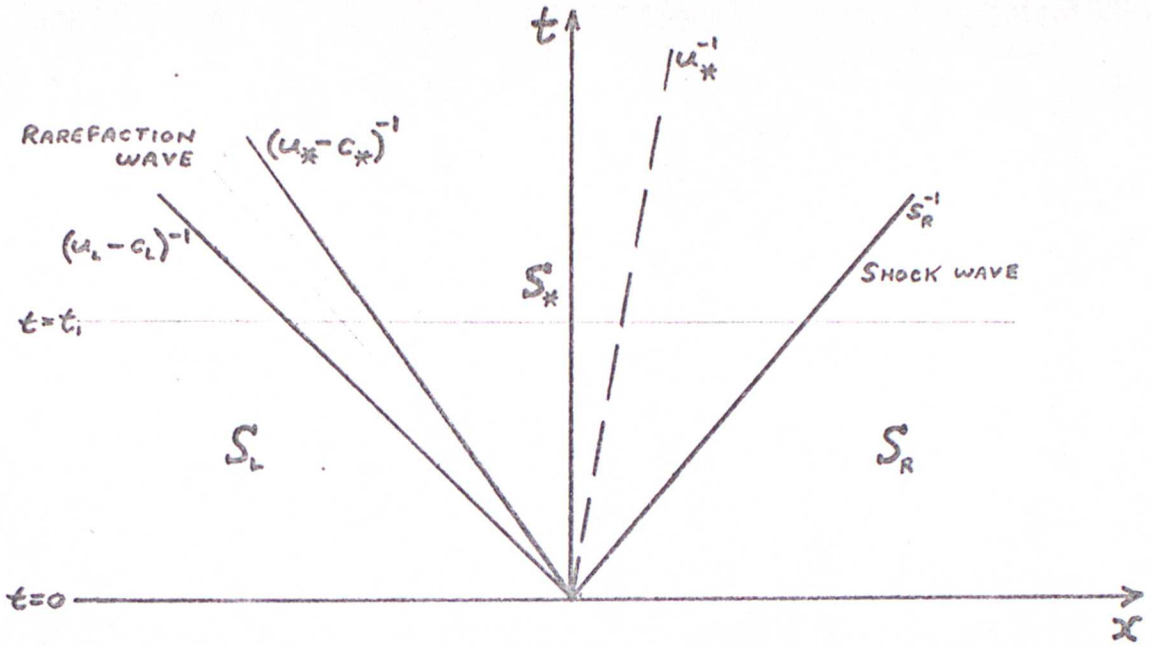

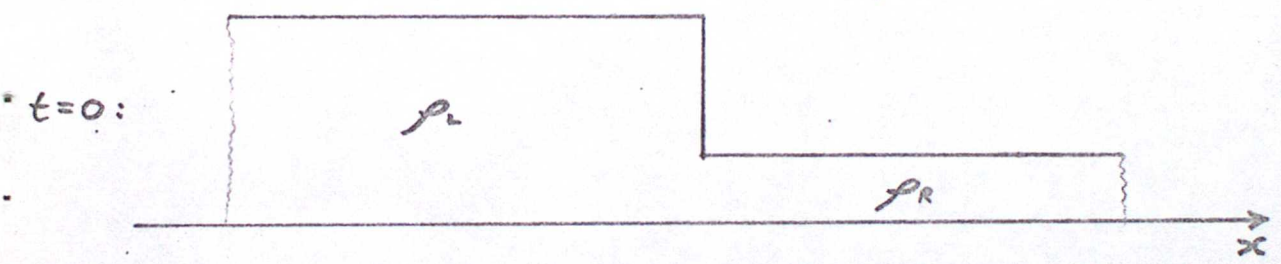

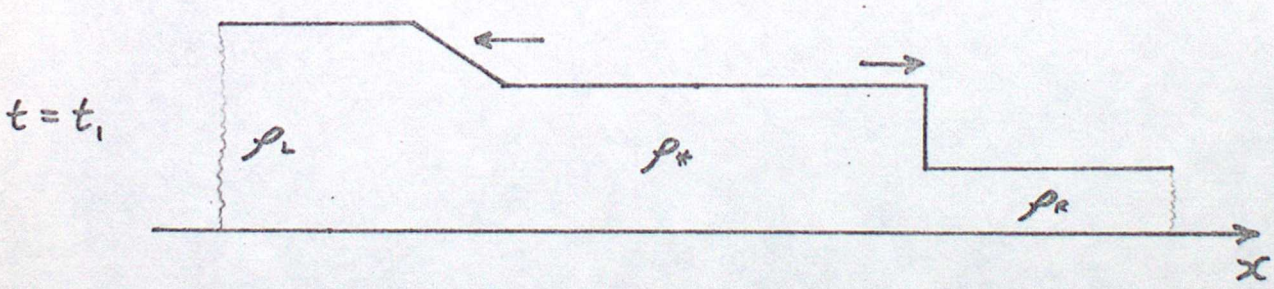

Figure 2. Solution of a Riemann problem with $\rho_L > \rho_R$: a shock-wave moving to the right and a rarefaction-wave moving to the left.

wave moving to the left. The three other possible combinations of waves (dependent on the initial conditions) are either two (compressive) shock waves, two rarefaction waves, or the situation opposite to Fig. 2 with the shock moving to the left and the rarefaction to the right. Other possibilities, for instance connecting S_L to S_* (in Fig. 2) with a rarefaction shock whose speed satisfied the jump conditions, are forbidden by the entropy condition and do not exist in nature. The entropy condition is needed to pick out the physically relevant solution, because weak solutions of conservation laws are not uniquely determined by their initial values. It requires that the fluid crossing a shock suffer an increase in entropy. Its shallow water analogy is the energy condition, which requires that fluid crossing a jump suffer a loss of energy, ie particles only move across a jump from a region of lower total depth to a region of higher total depth.

We now return to the Chorin-Godunov iterative procedure for the system (11), (12) together with equation (10). To solve the Riemann problem we need to evaluate u_* and P_* (or ρ_*) in the centre state S_*. We define the quantity $M_L = (P_L - P_*)/(u_L - u_*)$ (14). If the left wave is a shock, it can be shown using the jump condition $s_L[\rho] = [\rho u]$, that $M_L = \rho_L(u_L - s_L) = \rho_*(u_* - s_L)$ (15). Similarly, we define $M_R = (P_R - P_*)/(u_R - u_*)$ (16). If the right wave is a shock we obtain $M_R = -\rho_R(u_R - s_R) = -\rho_*(u_* - s_R)$ (17). For either of the two cases (14) or (15) for M_L and (16) or (17) for M_R we can obtain $M_R = (\rho_R P_R)^{1/2} F(P_*/P_R)$ (18), and $M_L = (\rho_L P_L)^{1/2} F(P_*/P_L)$ (19), where

$$\left.\begin{aligned} F(X) &= (X + X^{1/2})^{1/2} \quad , X \geq 1 \\ &= (1-X)/2\sqrt{2}(1-X^{1/4}) \, , X \leq 1 \end{aligned}\right\} \quad (20).$$

Upon elimination of u_* from (14) and (16), we obtain

$$P_* = \left(u_L - u_R + \frac{P_R}{M_R} + \frac{P_L}{M_L}\right)\Big/\left(\frac{1}{M_L} + \frac{1}{M_R}\right) \quad (21).$$

The three equations (18), (19) and (21) have three unknowns which can be found using an iterative procedure. To start the iteration, we choose an initial value for P_*, $P_*^0 = (P_R + P_L)/2$ (following Chorin), compute M_R^0 and M_L^0, and then compute P_*^{q+1}, M_R^{q+1} and M_L^{q+1} for $q \geq 0$ using

$$\bar{P}_*^q = (u_L - u_R + P_R/M_R^q + P_L/M_L^q)/(1/M_R^q + 1/M_L^q) \qquad (22a)$$

$$P_*^{q+1} = \alpha \max(\varepsilon 1, \bar{P}_*^q) + (1-\alpha) P_*^q \qquad (22b)$$

$$M_R^{q+1} = (P_R \rho_R)^{1/2} F(P_*^{q+1}/P_R) \qquad (22c)$$

$$M_L^{q+1} = (P_L \rho_L)^{1/2} F(P_*^{q+1}/P_L) \qquad (22d).$$

Equation (22b) serves two purposes: α is initially set equal to 1, and the first part of the right hand side is needed because there is no guarantee that in the course of the iteration P remains ≥ 0. We set $\varepsilon 1 = 10^{-6}$. The second term only comes into use if the iteration fails to converge (after L iterations), as may happen in the presence of a strong rarefaction (Chorin (1976)). To overcome this problem, α is halved after every L iterations (we set $L = 20$) until convergence is obtained. The iteration is stopped when

$$\max(|M_R^{q+1} - M_R^q|, |M_L^{q+1} - M_L^q|) \leq 10^{-6},$$

one then sets $M_R = M_R^{q+1}$, $M_L = M_L^{q+1}$ and $P_* = P_*^{q+1}$. To avoid spurious convergence when $P_L = P_R$, we ensured that the iteration was carried out at least twice.

After P_*, M_L and M_R have been determined we can obtain u_* by eliminating P_* from the definitions of M_L and M_R, to give

$$u_* = (P_L - P_R + M_L u_L + M_R u_R)/(M_L + M_R).$$

ρ_* is obtained from P_* using the relation $P = A\rho^\gamma$ (10a).

Now the complete solution to this simplified Riemann problem can be obtained using the jump conditions for shock waves and (since the flow is adiabatic in smooth

regions) the isentropic law and constancy of the Riemann Invariants for the rarefaction waves. This solution is then sampled at time $t_{n+1/2}$ at the points P_i.

Given the solution to the Riemann problem, the behaviour of this solution is largely determined by the values of θ_i (ie. the sampling positions, P_i). If θ_i is close to $-\frac{1}{2}$, the values of u and ρ at $((i+1/2)\Delta x, (n+1/2)\Delta t)$ will probably have come from S_L (i.e. $(i\Delta x, n\Delta t)$), while if θ_i is close to $\frac{1}{2}$, they will most likely have come from S_R. It is important that the θ_i tend as fast as possible to equidistribution on $[-\frac{1}{2}, \frac{1}{2}]$. If a new θ is picked for each i and each n, Chorin (1976) has shown that in general it produces an incorrect solution. This is because there is a finite probability that a given state will propogate to both left and right and create a spurious constant state. Thus, to prevent this happening, we chose a new value of θ only once per time level, θ^n. To further increase the rate at which θ^n reached equidistribution over $[-\frac{1}{2}, \frac{1}{2}]$, we used the following procedure suggested by Chorin (1976): the interval $[-\frac{1}{2}, \frac{1}{2}]$ was divided into m_2 sub-intervals, and $\bar{\theta}^1$ was chosen at random from the first subinterval, $\bar{\theta}^2$ from the second, ..., and $\bar{\theta}^{m_2+1}$ was chosen from the first subinterval again, and so-on. The sequence of $\bar{\theta}^n$ replaced the sequence of θ^n and were obtained using the formula

$$\bar{\theta}^n = (\ell_n + \theta^n + 1/2)/m_2 - 1/2 \ ,$$

where ℓ_n is an integer given by $\ell_{n+1} = (m_1 + \ell_n) \bmod (m_2)$, where $\ell_0 < m_2$; m_1 and m_2 are two mutually prime integers, $m_1 < m_2$. For the results presented here we used $m_1 = 3$, $m_2 = 7$ and $\ell_0 = 0$. We also tried a few runs with $m_2 = 11$, but there was no detectable difference in our results (beyond the inherent randomness).

For the computer implementation of the RCM, there are four main cases. If the sample point P_i lies to the right of the slip-line (i.e. $\bar{\theta}^n \Delta x > u_* \Delta t/2$)

we have two cases:

1. If $P_* > P_R$, the right wave is a shock; and (a) if P_i lies to the left of the shock line defined by $dx/dt = s_R$, we have $u = u_*$ and $\rho = \rho_*$; and (b) if P_i lies to the right of the shock line, we have $u = u_R$ and $\rho = \rho_R$.

2. If $P_* \leq P_R$, the right wave is a rarefaction wave. This is bounded on the left by the line defined by $\frac{dx}{dt} = u_* + c_*$, where $c_* = (\gamma P_*/\rho_*)^{1/2}$; and on the right by the line defined by $dx/dt = u_R + c_R$, where $c_R = (\gamma P_R/\rho_R)^{1/2}$. (a) If P_i lies to the left of the rarefaction wave, then $u = u_*$ and $\rho = \rho_*$; (b) if P_i lies to the right of it, then $u = u_R$ and $\rho = \rho_R$; and (c) if P_i lies inside the right rarefaction wave, we equate the slope of the C_+ characteristic, $\frac{dx}{dt} = u + c$, to the slope of the line through the origin and $(\bar{\theta}^n \Delta x, \Delta t/2)$, obtaining

$$u + c = 2\bar{\theta}^n \Delta x/\Delta t \qquad (23).$$

From the constancy of the J_- Riemann Invariant along the C_- characteristics (which cross the rarefaction),

$$u - 2c = u_R - 2c_R$$

$$\Rightarrow \quad c = c_R + \tfrac{1}{2}(u - u_R) \qquad (24)$$

and substituting into (23), we obtain

$$u = \tfrac{1}{3}\left(u_R - 2c_R + 4\frac{\bar{\theta}^n \Delta x}{\Delta t}\right) \qquad (25)$$

By substituting (25) back into (24), we can obtain c, which is then used to evaluate ρ, using

$$c = (\gamma P/\rho)^{1/2} \quad \text{and} \quad P = A\rho^{\gamma}.$$

The other two cases, with P_i lying to the left of the slip-line, and the left wave being either a shock or a rarefaction wave, are mirror images of cases 1 and 2, with C_+, J_- replaced by C_-, J_+, and will not be described in detail (see Sod (1978) for full details and a flow diagram).

To obtain the solution for v (or n), we solved equation (7) in the form

$$\frac{\partial v}{\partial t} + u \frac{\partial v}{\partial x} = 0 \qquad (7a).$$

It can be found from the jump conditions for equations (6), (7) and (8) (ie $s[\underline{w}] = [\underline{F}(\underline{w})]$, where (6), (7), (8) have been written in the form $\frac{\partial \underline{w}}{\partial t} + \frac{\partial}{\partial x}\underline{F}(\underline{w}) = 0$), that v is continuous across a jump in ϕ and u, although it may be discontinuous across a contact discontinuity, and initially we assumed that it was. Thus equation (7a) was firstly solved for piecewise constant v, with $v_{i+\frac{1}{2}}^{n+\frac{1}{2}}$ taking the value of either v_L or v_R depending on the x-component of velocity $u_{i+\frac{1}{2}}^{n+\frac{1}{2}}$; ie in an $x-t$ diagram the sample point P_i (at time $t_{n+\frac{1}{2}}$) was traced back to time t_n along the line with slope $(u_{i+\frac{1}{2}}^{n+\frac{1}{2}})^{-1}$, then if this position (P_i^n) was to the left of the contact discontinuity position at time t_n, $(i+\frac{1}{2})\Delta x$, $v_{i+\frac{1}{2}}^{n+\frac{1}{2}}$ took the value of v_L, and if P_i^n was to the right of $(i+\frac{1}{2})\Delta x$, $v_{i+\frac{1}{2}}^{n+\frac{1}{2}}$ took the value of v_R. Unfortunately, using this representation of v, it was found that spurious constant states were generated, which lead to errors in the profiles of u and ϕ. So, to overcome this, we made v piecewise linear between the values at the grid-points (for odd-numbered half-time-steps; and linear between intermediate points for even-numbered half-time-steps – due to the staggered grid used in the RCM). We then sampled v at the intermediate points $(i+\frac{1}{2})\Delta x$ (for which we are looking for the solution), assuming that the appropriate value of v^n travelled along the x-axis with the velocity $u^{n+\frac{1}{2}}$ found at this point $(i+\frac{1}{2})\Delta x$ (instead of with $u_{i+\frac{1}{2}}^{n+\frac{1}{2}} \equiv u^{n+\frac{1}{2}}(P_i)$, as previously). This involved sampling the new u-profile at the point $(i+\frac{1}{2})\Delta x$ (see Fig. 3). This had the desired effect of producing a smoother v-profile and thus prevented the formation of any spurious constant states. Removing the randomness from this part of the sampling procedure was justified, because it was introduced to deal with discontinuities and v was not discontinuous.

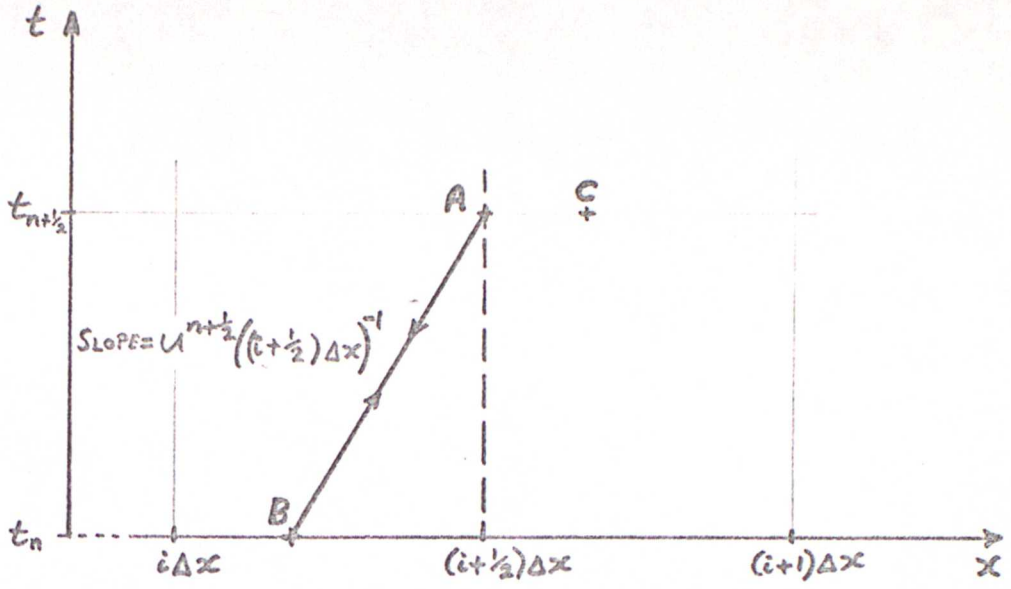

A = the fixed sampling point for v, $(i+\frac{1}{2})\Delta x$, at time $t_{n+\frac{1}{2}}$;

B = the point P_i^n, from which the value of v was taken forward to time $t_{n+\frac{1}{2}}$;

C = the random sampling point for u and ρ, P_i.

Figure 3. Illustrating the sampling procedure for v.

Once the initial values of u and v had been obtained, as described above, they were then adjusted to take into account the effect of rotation. This was done by simply rotating the velocity vector $\underline{v} = (u, v)$ through an angle of $f\Delta t/2$ at each half-time-step (this method of adjustment ensured that $|\underline{v}|$ was not changed).

3. The Finite Difference Methods

(a) Firstly, the equations (1), (2), (3) were re-written in the following flux form:

$$\left.\begin{aligned} &\frac{\partial}{\partial t}(\phi u) + \frac{\partial}{\partial x}\left(u^2\phi + \tfrac{1}{2}\phi^2\right) - f\phi v - K\frac{\partial^2}{\partial x^2}(\phi u) = 0 \\ &\frac{\partial}{\partial t}(\phi v) + \frac{\partial}{\partial x}(\phi u v) + f\phi u - K\frac{\partial^2}{\partial x^2}(\phi v) = 0 \\ &\frac{\partial}{\partial t}\phi + \frac{\partial}{\partial x}(\phi u) - K\frac{\partial^2}{\partial x^2}\phi = 0 \end{aligned}\right\} \quad (26)$$

where artificial viscosity (or diffusion) terms have also been added to the equations (and K is the diffusion coefficient). These were then solved numerically by discretising them into the form:

$$m_i^{n+1} = m_i^{n-1} - 2\Delta t\left\{\frac{(u_{i+1}^n + u_i^n)(m_{i+1}^n + m_i^n) - (u_i^n + u_{i-1}^n)(m_i^n + m_{i-1}^n)}{4\Delta x} + \frac{\phi_{i+1}^{n^2} - \phi_{i-1}^{n^2}}{4\Delta x} - f n_i^n - K\frac{(m_{i+1}^{n-1} - 2m_i^{n-1} + m_{i-1}^{n-1})}{\Delta x^2}\right\}$$

$$n_i^{n+1} = n_i^{n-1} - 2\Delta t\left\{\frac{(v_{i+1}^n + v_i^n)(m_{i+1}^n + m_i^n) - (v_i^n + v_{i-1}^n)(m_i^n + m_{i-1}^n)}{4\Delta x} + f m_i^n - K\frac{(n_{i+1}^{n-1} - 2n_i^{n-1} + n_{i-1}^{n-1})}{\Delta x^2}\right\} \quad (27)$$

$$\phi_i^{n+1} = \phi_i^{n-1} - 2\Delta t\left\{\frac{(m_{i+1}^n - m_{i-1}^n)}{2\Delta x} - K\frac{(\phi_{i+1}^{n-1} - 2\phi_i^{n-1} + \phi_{i-1}^{n-1})}{\Delta x^2}\right\}$$

where $\phi_i^n \equiv \phi(i\Delta x, n\Delta t)$, $m_i^n \equiv (\phi u)_i^n$ and $n_i^n \equiv (\phi v)_i^n$; and where we have used centred time differences, except for the diffusion terms, which were forward-differenced in order to ensure stability (and obviously forward time-differences were used for the first time-step for all terms).

(b) Secondly, the equations (1), (2), (3) were solved as they stand, except for the addition of artificial diffusion terms, to see if a non-"conservation" form of the equations would give the correct (or at least similar) solution. So, the equations solved were:

$$\left.\begin{aligned} &\frac{\partial u}{\partial t} + u\frac{\partial u}{\partial x} + \frac{\partial \phi}{\partial x} - fv - K\frac{\partial^2 u}{\partial x^2} = 0 \\ &\frac{\partial v}{\partial t} + u\frac{\partial v}{\partial x} + fu - K\frac{\partial^2 v}{\partial x^2} = 0 \\ &\frac{\partial \phi}{\partial t} + u\frac{\partial \phi}{\partial x} + \phi\frac{\partial u}{\partial x} - K\frac{\partial^2 \phi}{\partial x^2} = 0 \end{aligned}\right\} \quad (28)$$

These were discretised into the form:

$$u_i^{n+1} = u_i^{n-1} - 2\Delta t\left\{\frac{(u_{i+1}^{n\,2} - u_{i-1}^{n\,2})}{4\Delta x} + \frac{(\phi_{i+1}^n - \phi_{i-1}^n)}{2\Delta x} - fv_i^n - K\frac{(u_{i+1}^{n-1} - 2u_i^{n-1} + u_{i-1}^{n-1})}{\Delta x^2}\right\}$$

$$v_i^{n+1} = v_i^{n-1} - 2\Delta t\left\{\frac{(u_{i+1}^n + u_i^n)(v_{i+1}^n - v_i^n) + (u_i^n + u_{i-1}^n)(v_i^n - v_{i-1}^n)}{4\Delta x} + fu_i^n - K\frac{(v_{i+1}^{n-1} - 2v_i^{n-1} + v_{i-1}^{n-1})}{\Delta x^2}\right\} \quad (29)$$

$$\phi_i^{n+1} = \phi_i^{n-1} - 2\Delta t\left\{\frac{(u_{i+1}^n \phi_{i+1}^n - u_{i-1}^n \phi_{i-1}^n)}{4\Delta x} - K\frac{(\phi_{i+1}^{n-1} - 2\phi_i^{n-1} + \phi_{i-1}^{n-1})}{\Delta x^2}\right\}$$

4. Numerical Results

The initial fields for all the experiments were given by

$$u(x,0) = U\cos(x/L),$$

$$v(x,0) = 0,$$

$$\phi(x,0) = \phi_m + U\left\{\frac{U}{8}\cos(2x/L) + (\phi_m - \frac{U^2}{8})^{1/2}\cos(x/L)\right\},$$

where the length of the domain $= 2\pi L$, $\phi_m = gh_m$, and h_m = the mean height of the fluid. These are the same as those used in WH, and they are shown in Fig. 6. Periodic boundary conditions were enforced; and $\Delta x = 2\pi L/N$, where $N = 320$ for most experiments. Following WH, the numerical results presented here are in the

form of profiles of the non-dimensional variables $u' = u/U$, $v' = v/U$ and $h' = (\phi - \phi_m)/U\phi_m^{1/2}$. For the two different cases presented, the initial Froude number F was the same, $F = U/\phi_m^{1/2} = 1.0$.

Figures 4 and 5 show a comparison between the finite difference method (a), using the flux form of the equations, and the RCM, for the case where $R_o = 0.1$, in which jumps were prevented from forming by the action of the Coriolis force. The time is given in units of the inertial time scale f^{-1} , and 320 grid-points were used (N = 320). As noted by WH, there is an inertial oscillation present, with period $2\pi f^{-1}$. There was little change in the shape of the height profile, h, throughout this oscillation. The time shown here is $ft = 3\pi/2$, i.e. $\frac{3}{4}$ of the way through the cycle. We can see that the RCM produced a much less smooth set of profiles than the F.D. method (which will give the correct solution in the absence of discontinuities). This was due to the random sampling in the RCM; which is only first order accurate. The general shapes of the profiles from the two methods were very close throughout the oscillation. With twice the number of points the profiles were even closer. This shows us that the RCM does tend towards the correct solution for fields that remain smooth; although quite a large number of points are required in order to reduce the roughness of the profiles to an acceptable level. Also, the RCM is much less economical to use than the F.D. method, for the same number of grid-points; as can be seen from the CPU times required to complete the inertial oscillation partially shown in Figs. 4 and 5: 3.1 seconds for the F.D. method and 72.0 seconds for the RCM (both were run on the IBM 360/195).

The formation and subsequent evolution of a hydraulic jump is shown in Figs 6–10 (for the RCM model), for the case with $R_o = 1.0$. The time is given in units of the advective time-scale L/U, which is the same as the inertial time-scale here with $R_o = U/fL = 1.0$; and N = 320. In this case rotation was still present, but it was not dominant as it was for the case with $R_o = 0.1$,

and it was unable to prevent the formation of a jump. As with WH's results with their F.D. method (displayed in their Fig. 1), the jump had formed by $Ut/L = 0.7$. Then, we can see that it sharpened and travelled forward (in the +ve x-direction), and simultaneously a trough formed in h behind the jump, resulting in a sharp "spike" in the h-profile at the jump (as seen in Fig. 8 at $Ut/L = 1.4$). Also, the v-profile developed a sharp discontinuity in slope at the jump. By $Ut/L = 2.1$ (Fig. 9) the jump had propagated further along the x-axis, as the spike in h moved up the slope which was ahead of the jump, and the trough behind the jump continued to propagate in the -ve x-direction. The jump in u, which reached a maximum near $Ut/L = 1.4$, had decreased somewhat by $Ut/L = 2.1$, and the value of u over all x had decreased (or become more negative). Meanwhile, the v-profile had developed a more marked minimum behind the jump, due to the action of the Coriolis force on the earlier high values of u behind the jump. The maximum in v can be seen to have occurred at the jump rather than ahead of it, presumably because the jump was moving to the right and so overtaking and absorbing any smooth maximum in v that tried to form. The maximum in v had broadened (behind the jump) by $Ut/L = 2.8$ (Fig. 10), and this seems to be associated with a slight broadening of the spike in h, which was presumably due to the interaction of the jump with the wave travelling in the opposite direction. The jump itself had continued to propagate forwards with no dissipation, as expected with this method.

If we now compare Fig. 10 with Fig. 11, which is from another run of the RCM model with the same parameters, but a different set of random numbers, we can see that the results are reproducible up to this time. Only minor differences result from the different random numbers. In fact the results are reproducible up to at least $Ut/L = 5.6$.

The results from the F.D. model (a) for this time ($Ut/L = 2.8$), with the same number of grid-points, are shown in Fig. 12. The diffusion coefficient used here was $K = 2.5 \times 10^4 \ m^2 \ s^{-1}$. We can see that the profiles are very

similar to those produced by the RCM model (Figs. 10 and 11), as they were indeed for all the times up to $Ut/L = 5.6$. Although, naturally there was some smoothing of the jump over about 5 or 6 grid-lengths due to the artificial diffusion introduced. The value of K used here was chosen as the minimum that was able to quickly damp out the spurious oscillations produced behind the jump by the F.D. method. Larger values of K naturally produced a much more smoothed and less sharp jump; whereas lower values produced a sharper jump more akin to the RCM solution, but with oscillations behind it, which increased in magnitude and extent as K was decreased (although once formed, the oscillations did not grow in extent with time and decreased in magnitude due to the continued damping).

As with the no-jump case, the RCM results are seen to be "rough" compared to the smooth F.D. results, due to the random sampling procedure. There were also some small differences in the positions of the jump from different RCM runs, but this was to be expected (MM) (again due to the randomness), and on the average the positions were the same as those from the F.D. runs. Thus, the RCM model's solution does tend (on average) towards that of the F.D. model. So, assuming that our adaption of the RCM gives the correct solution, then our conventional F.D. method (a), using the flux form of the equations, also gives the correct solution.

Figures 13, 14 and 15 show results of further runs of the F.D. model (a), with different numbers of grid-points. The value of K was changed for each run to ensure that the same scales were damped each time. With higher resolution (Fig. 13, N = 640), the jump is naturally sharper, but otherwise the profiles are virtually identical to those in Fig. 12, with just a slight sharpening of the trough in v behind the jump. As the resolution was decreased to N = 160 (Fig. 14), the jump (and "spike") was naturally smoothed out more, resulting in a reduction in amplitude in h of about 10%; also, due to the smoothing of

the jump, its mean position is seen to be slightly further back (although the front of the jump is at the same place), and the profiles behind the jump are somewhat different (mostly due to the smoothing of the trough). As the resolution was reduced further to N=40, we can see from Fig. 15 that the jump was smoothed out so much that it is hardly recognisable as a jump, although the jump region still occupies only 4 or 5 grid-lengths (which is the same as for N = 160); the remaining parts of the profiles were also smoothed considerably, and the general evolution seems to be slightly slower.

Figure 16 shows an example of the results from F.D. model (b), ie. the one using a non-conservation form of the equations. We can see immediately that it is seriously in error compared to both F.D. model (a) and the RCM model. The jump is seen to have propagated much slower and is considerably reduced in amplitude. Also, there are quite large discrepancies in the velocity profiles, in particular the u-profile behind the jump (a spurious bulge). The error in jump position seems to have been the result of the jump moving much more slowly just after it had formed, and this was associated with lower values of the u-component of velocity behind the jump (evident at $Ut/L = 1.4$). There was also a much shallower trough in h behind the jump at this time, compared to the other two models. From $Ut/L = 2.1$ onwards (up to $Ut/L = 5.6$) the errors do not seem to have increased, since the jump position remained approximately the same distance in error and no more major discrepancies developed in the shapes of the profiles.

5. Summary and Discussion

The Random Choice Method, as used by Marshall and Mendez (1981) to model numerically the one-dimensional shallow-water equations, has been modified here to include rotation. After establishing that this modified numerical model gave the correct solution for a smooth (high rotation-rate) case, it was then

applied to a low rotation-rate case in which a hydraulic jump developed. The evolution of the jump in this model was compared with its evolution in a conventional F.D. model incorporating artifical diffusion. It had been suspected that the F.D. model might have given somewhat different results in the vicinity of the jump, soon after it had formed, which could have subsequently corrupted the solution. In terms of characteristics, it is well known for the case with no rotation that the artifical diffusion incorporated into the F.D. model has the effect of preventing characteristics of the same family from meeting and forming a discontinuous jump; they just come closer together with time. With rotation in the model, it had been thought that possibly the characteristics diverged again, rather than continuing to slowly converge, and that they then carried information away from the jump region as spurious wave packets, dissipating the jump. From our results here, it seems that this was not the case, with the F.D. model giving the correct solution (with the optimum diffusion), but with some smoothing if the resolution was too low. When the non-conservative formulation of the equations was used, errors were found soon after jump formation; as also occurs without rotation.

This work is going to be extended to include jumps forced by orography, in order to see whether F.D. models can correctly handle the evolution of the jumps in this case.

6. References

1. A J Chorin, "Random Choice Solution of Hyperbolic Systems", Journal of Computational Physics, Vol. 22, 1976, 517-533.

2. A J Chorin and J E Marsden, "Mathematical Introduction to Fluid Mechanics", Springer-Verlag, New York/Berlin, 1979.

3. J Glimm, "Solutions in the Large for Nonlinear Hyperbolic Systems of Equations", Communications on Pure and Applied Mathematics, Vol. 18, 1965, 697.

4. S K Godunov, "A Finite Difference Method for the Numerical Computation of Discontinuous Solutions of the Equations of Fluid Dynamics", Mat. Sbornik, Vol. 47, 1959, 271.

5. G Marshall and R Mendez, "Computational Aspects of the Random Choice Method for Shallow Water Equations", Journal of Computational Physics, Vol. 39, 1981, 1-21.

6. G A Sod, "A Survey of Several Finite Difference Methods for Systems of Nonlinear Hyperbolic Conservation Laws", Journal of Computational Physics, Vol. 27, 1978, 1-31.

7. R T Williams and A M Hori, "Formation of Hydraulic Jumps in a Rotating System", Journal of Geophysical Research, Vol. 75, No. 15, 1970, 2813-2821.

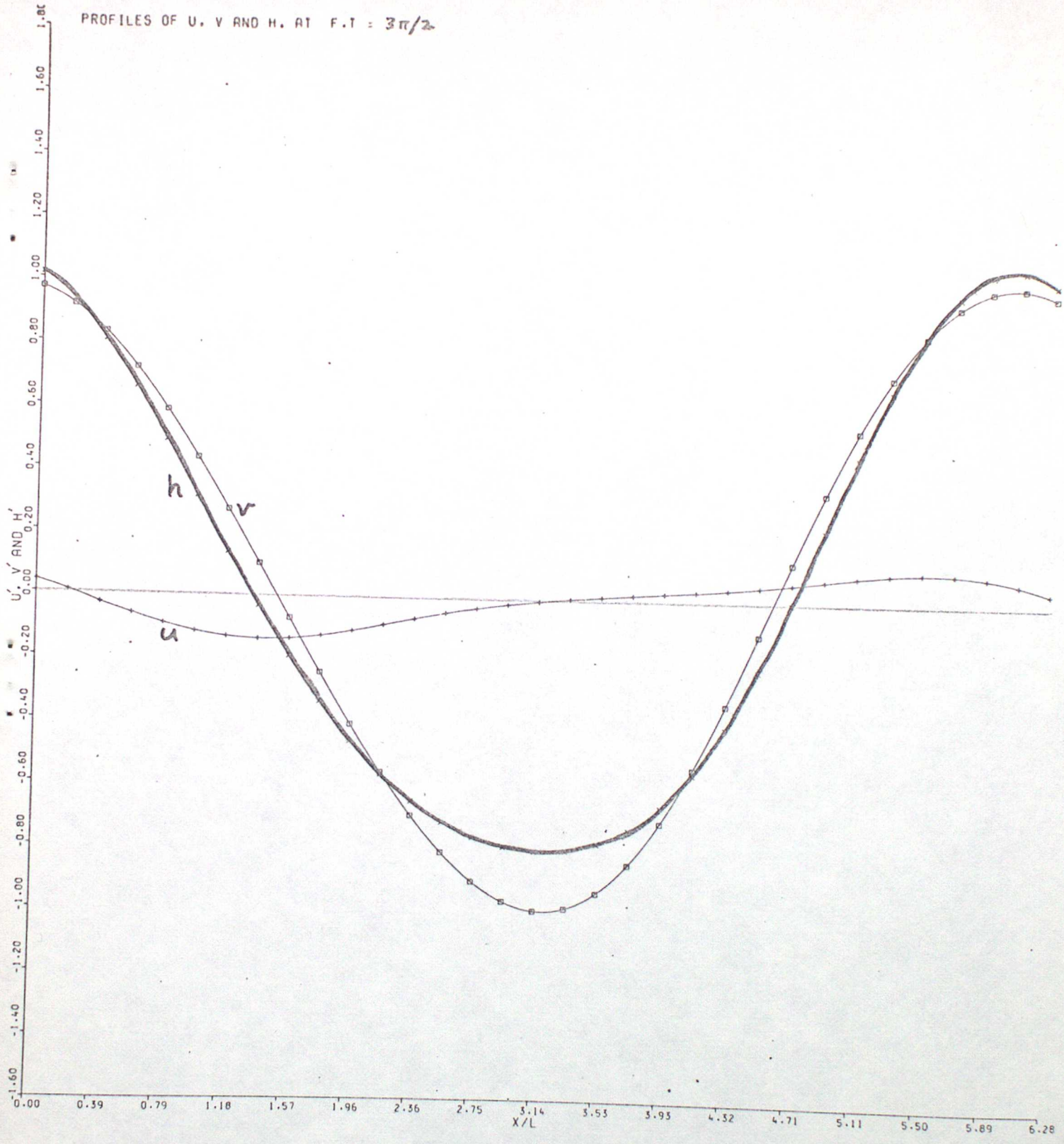

Figure 4. Finite Difference method (a), for $R_e=0.1$ (smooth solution), at "time" $ft=3\pi/2$.

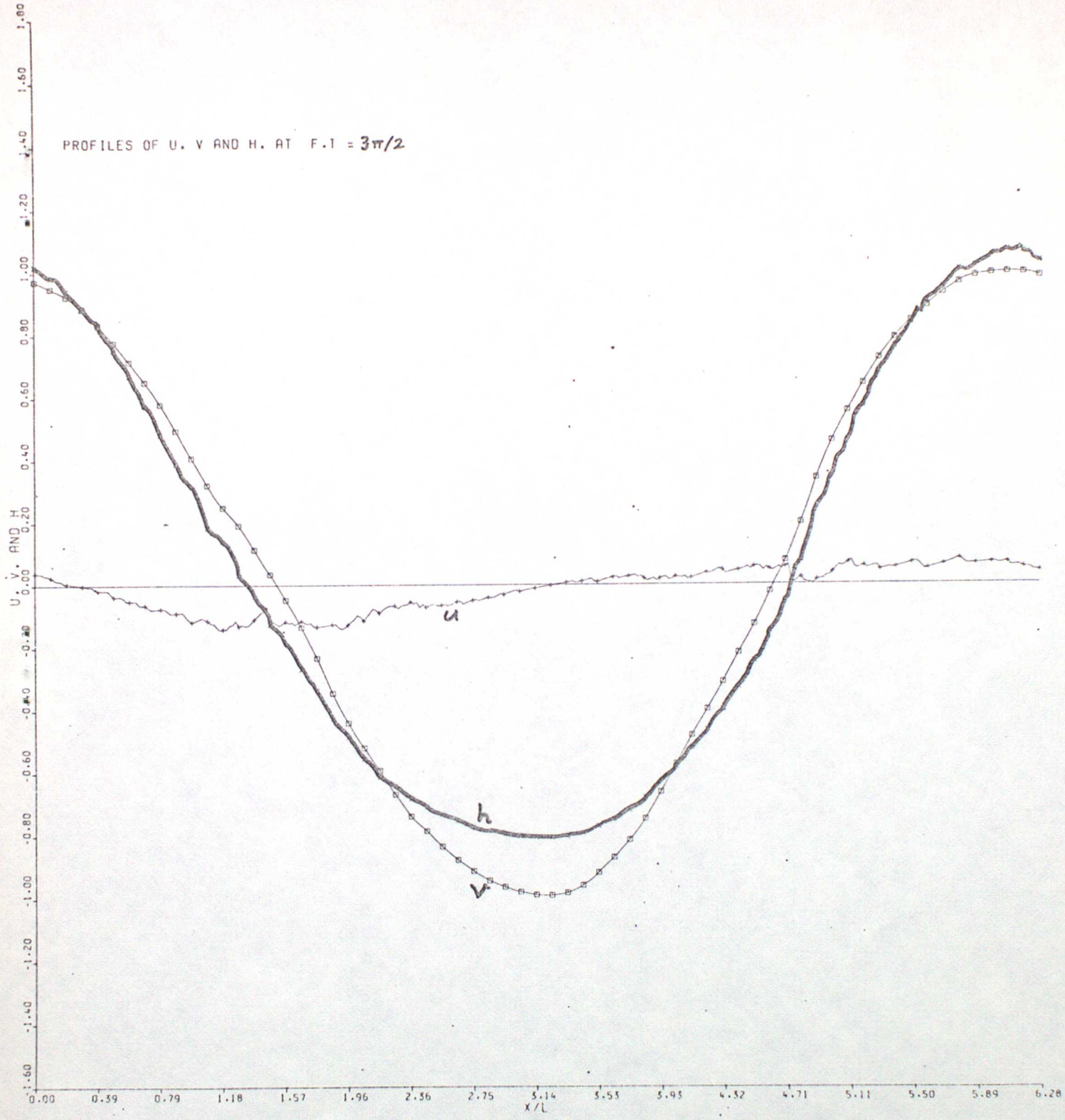

Figure 5. RCM for same case as shown in Fig. 4 .

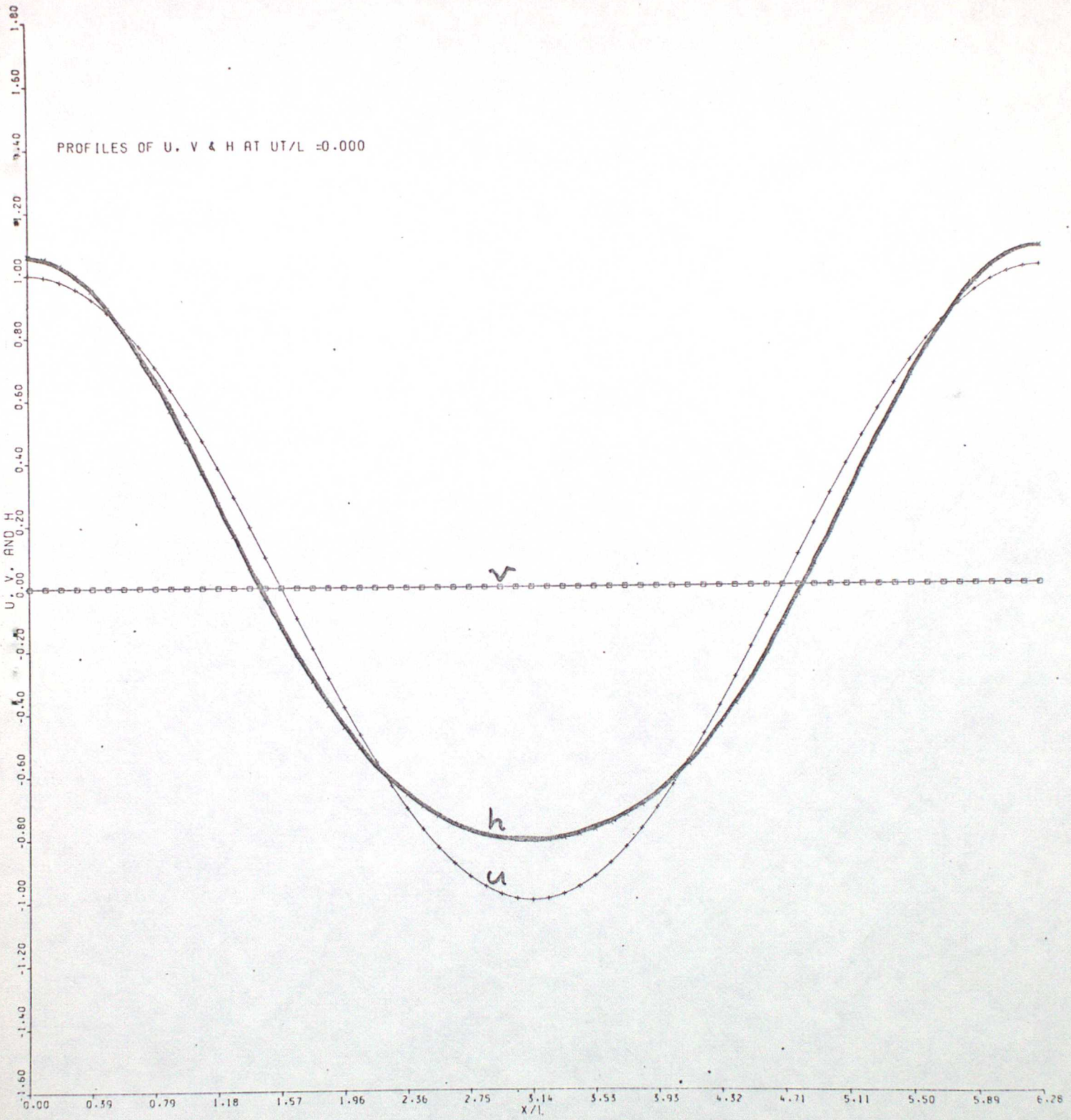

Figure 6. RCM solution for a case with R_o=1.0, at "time" Ut/L=0.

N = 320.

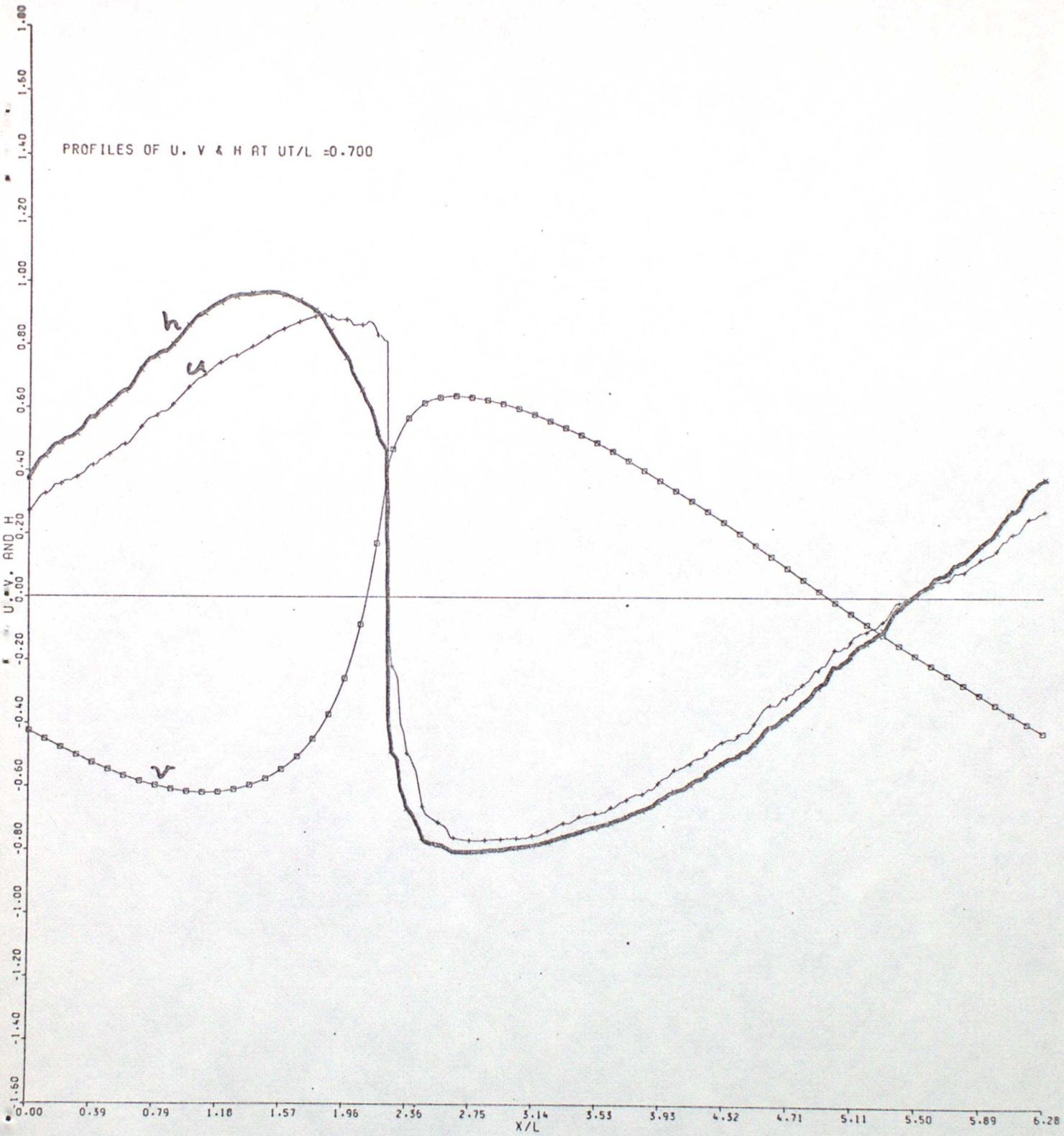

Figure 7. As Fig. 6, at Ut/L=0.7.

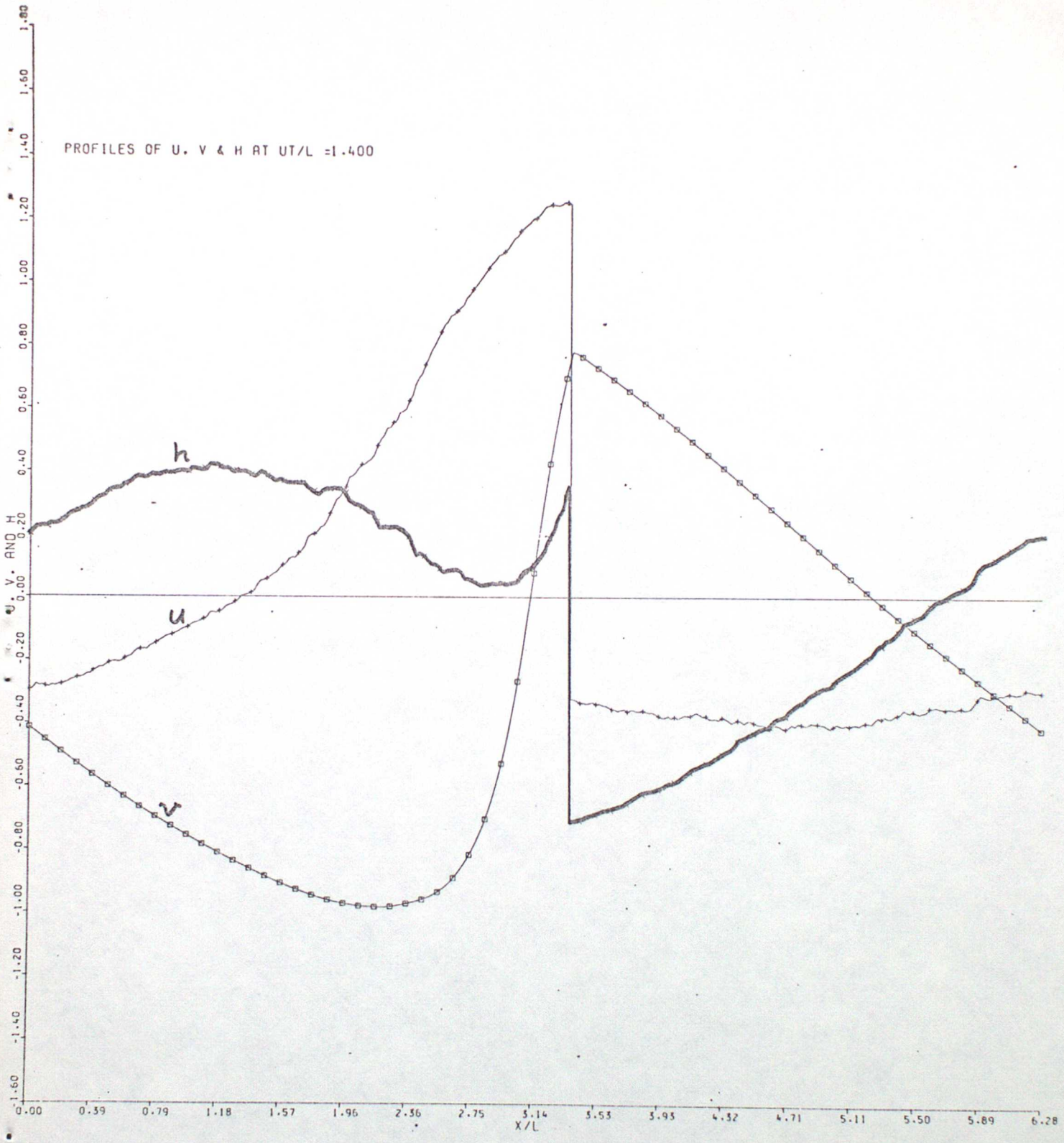

Figure 8. As Fig. 6, at Ut/L = 1.4.

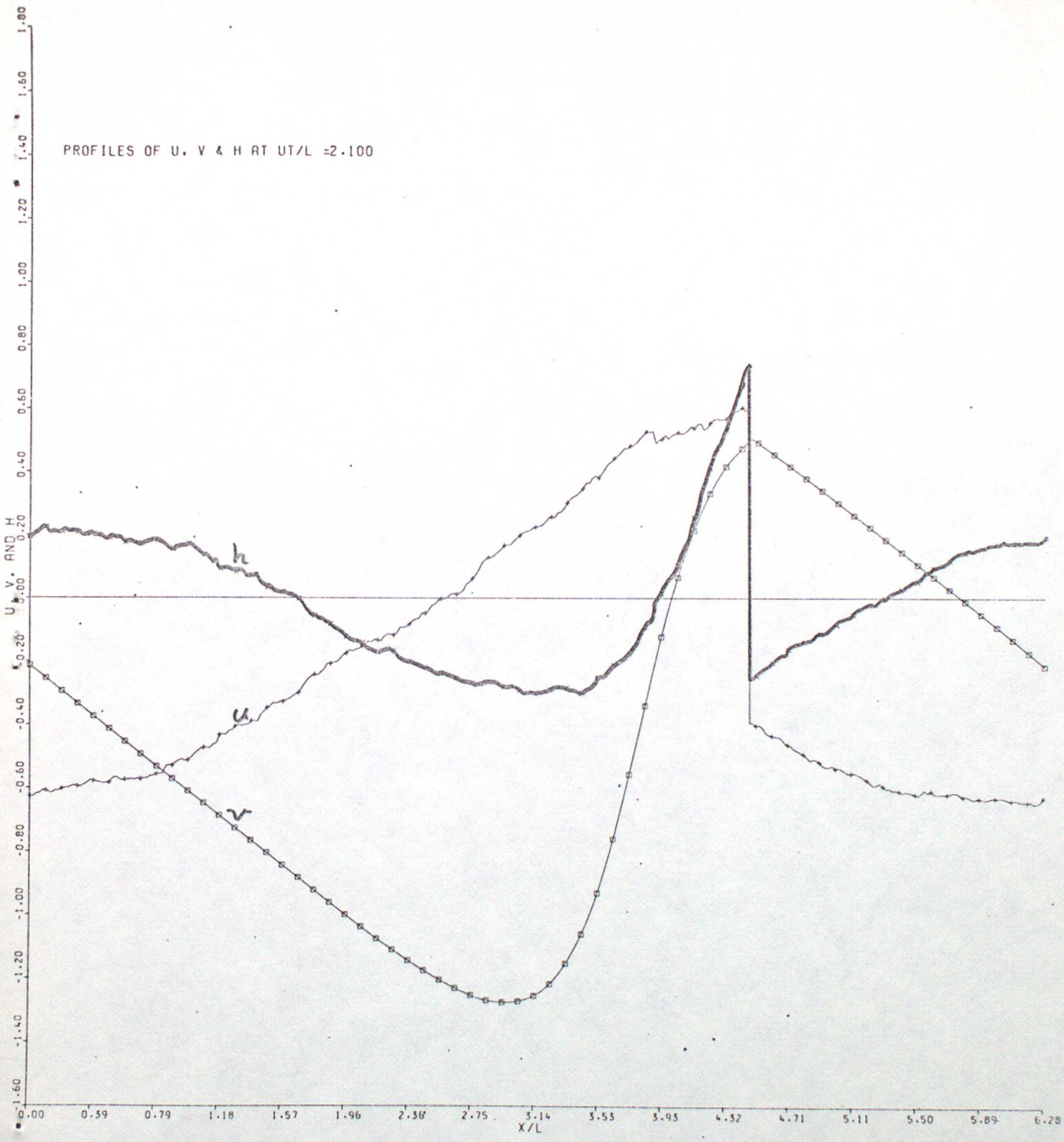

Figure 9. As Fig. 6, at Ut/L = 2.1.

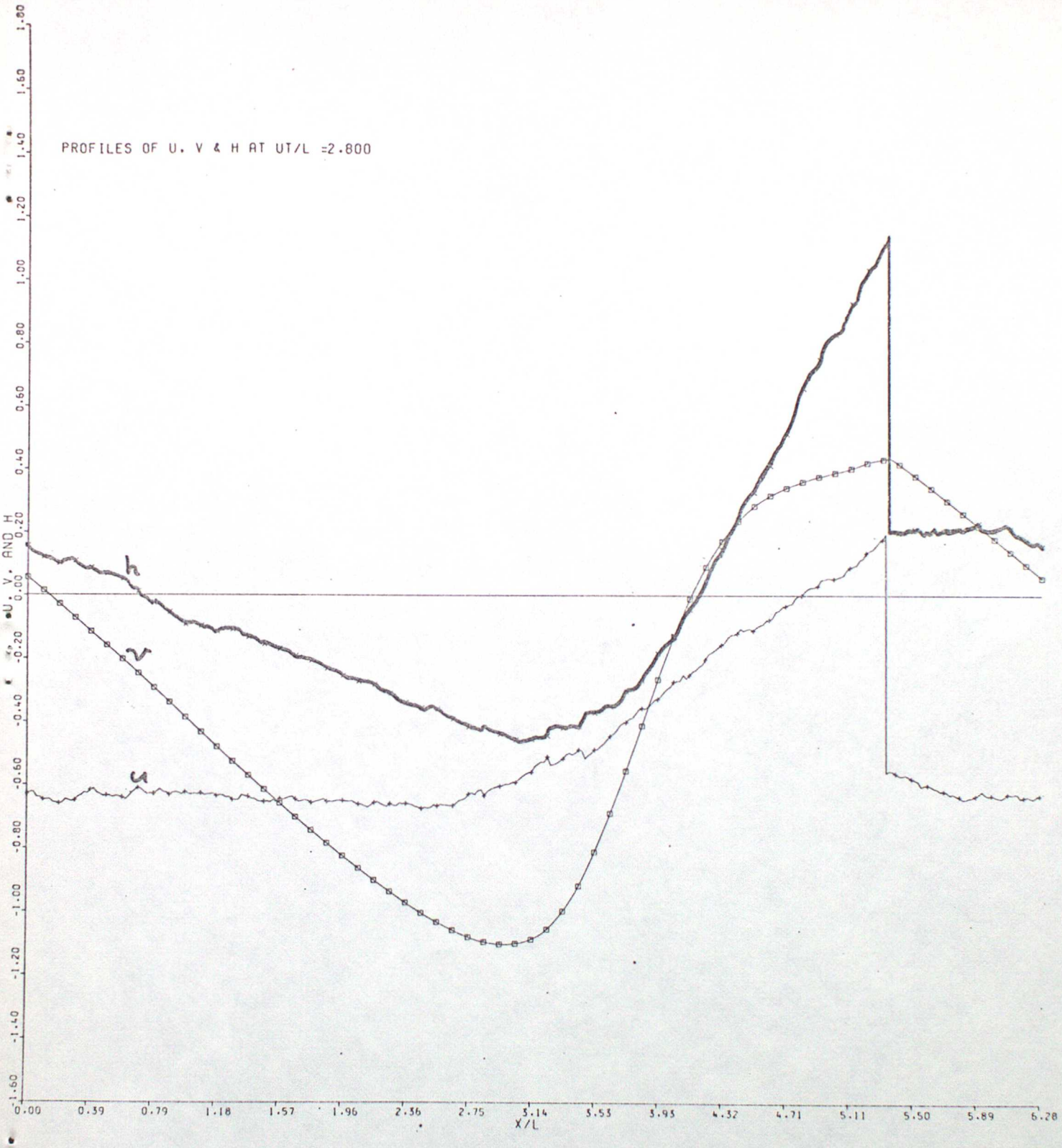

Figure 10. As Fig. 6, at Ut/L = 2.8.

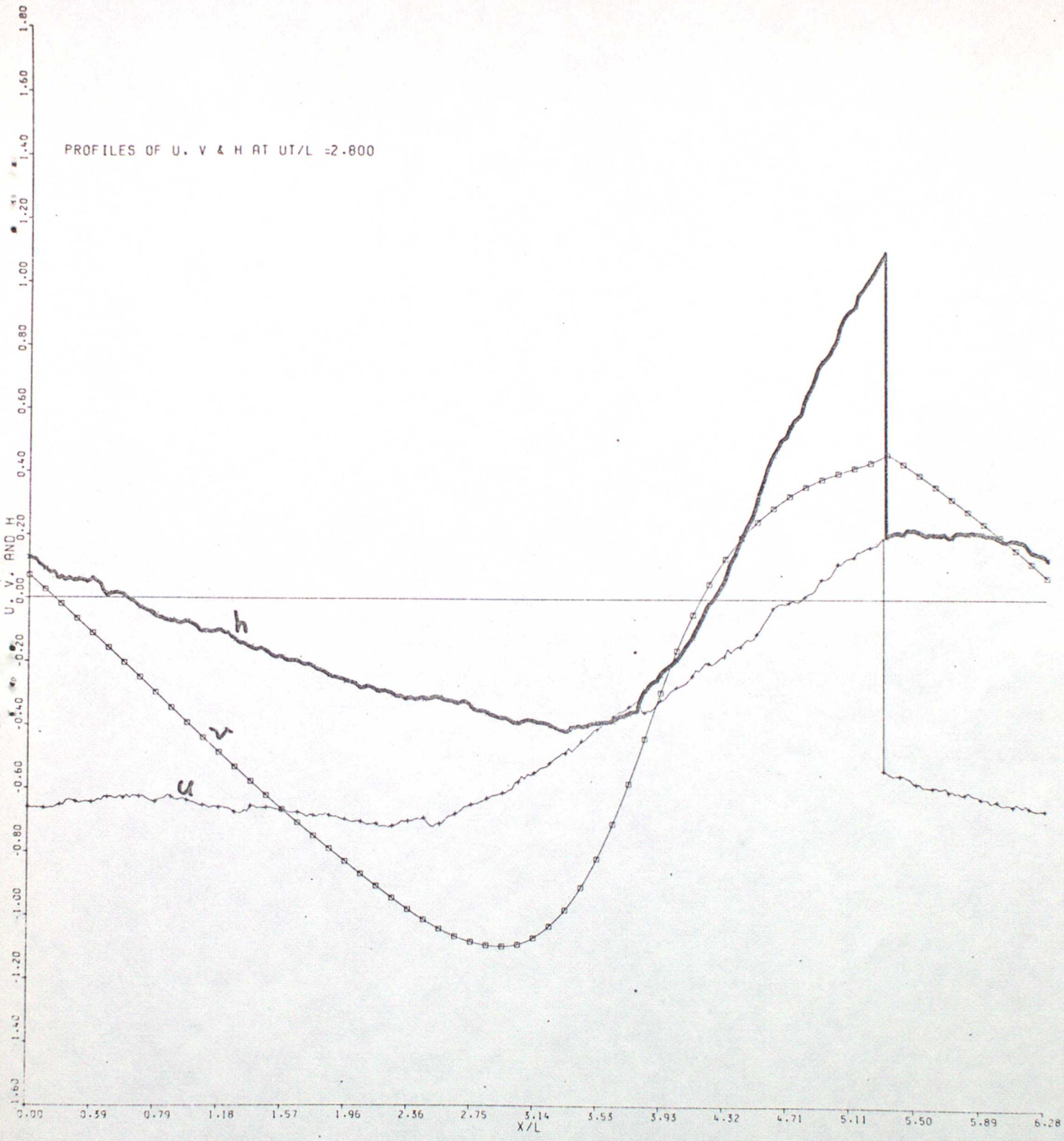

Figure 11. As Fig. 10, but for another run of the RCM model with different random numbers.

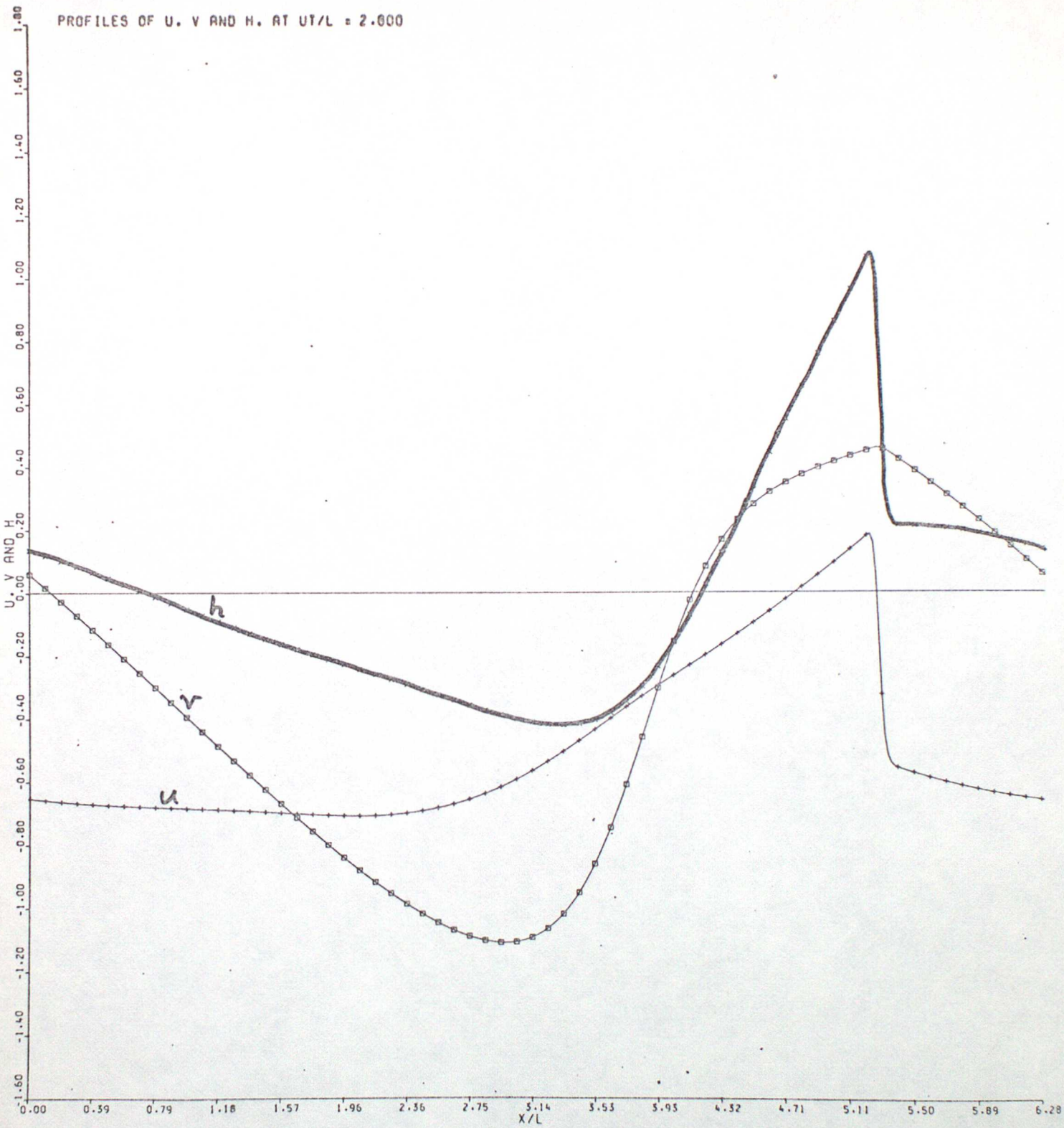

Figure 12. Results from F.D. model (a), at Ut/L =2.8.

N =320, K = 2.5×10^{4} $m^2 s^{-1}$.

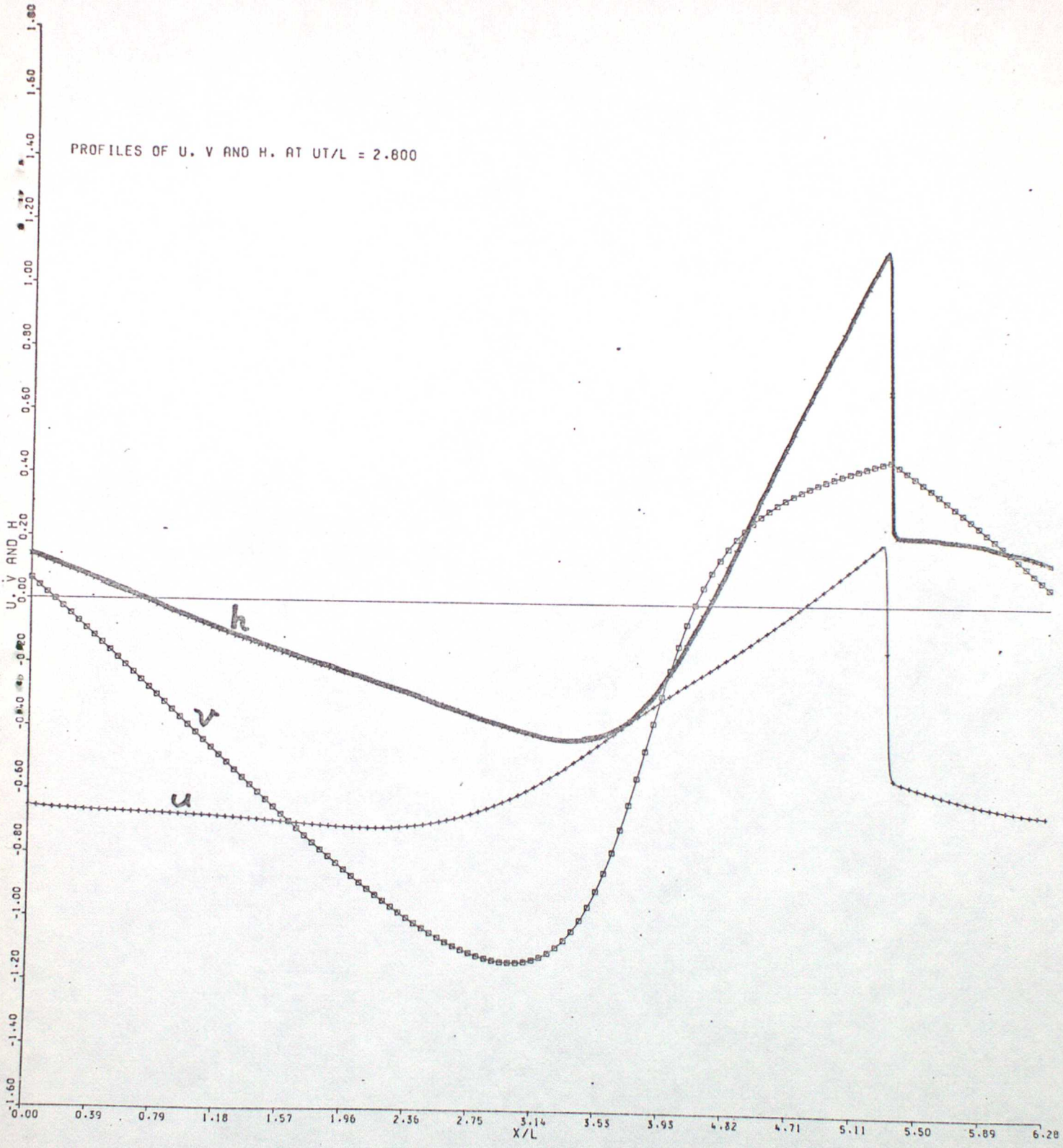

Figure 13. As Fig. 12, but with N = 640 and K = 1.25×10^{4} $m^{2}s^{-1}$.

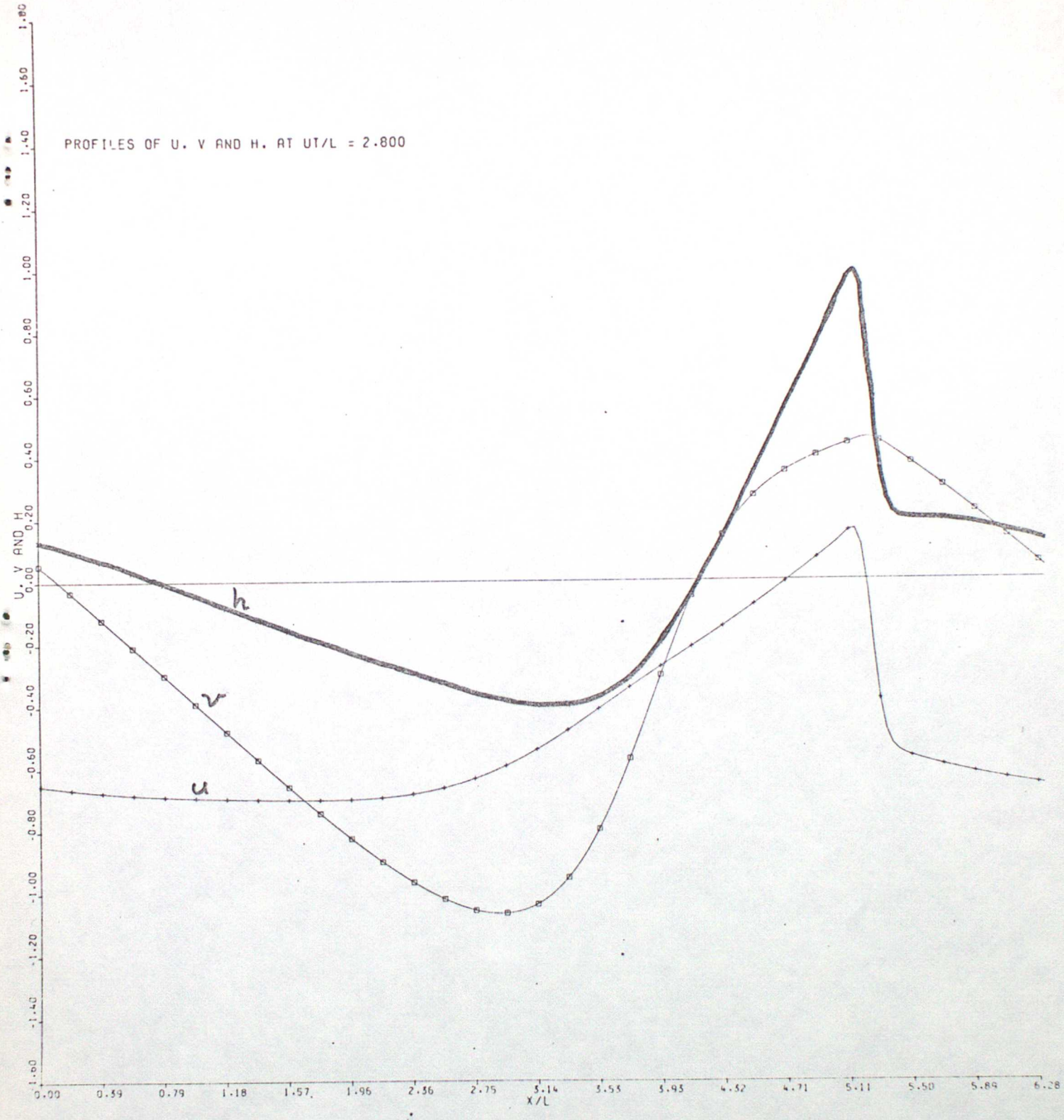

Figure 14. As Fig. 12, but with N = 160 and K = 5×10^{4} $m^2 s^{-1}$.

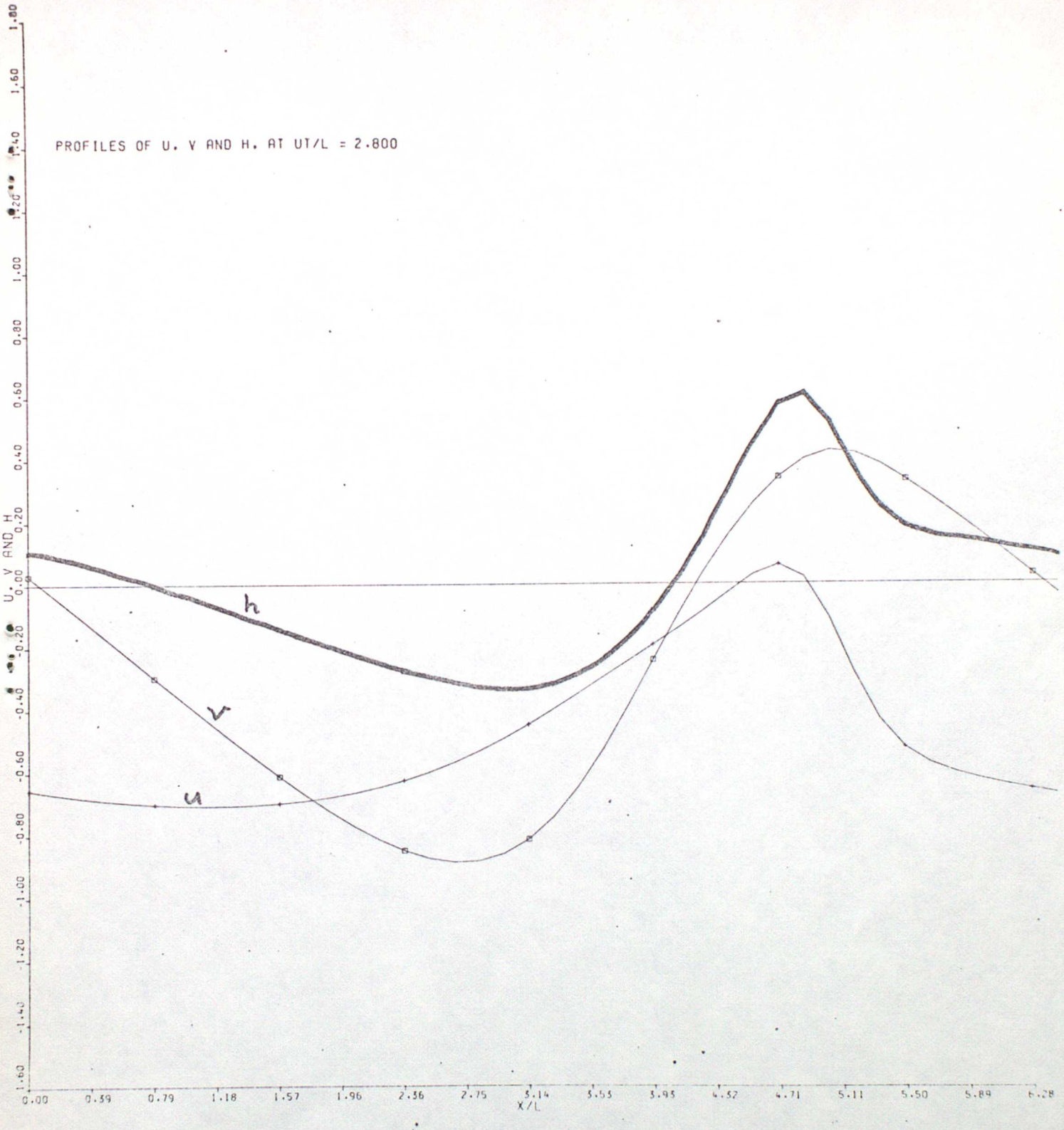

Figure 15. As Fig. 12, but with $N = 40$ and $K = 10^5$ $m^2 s^{-1}$.

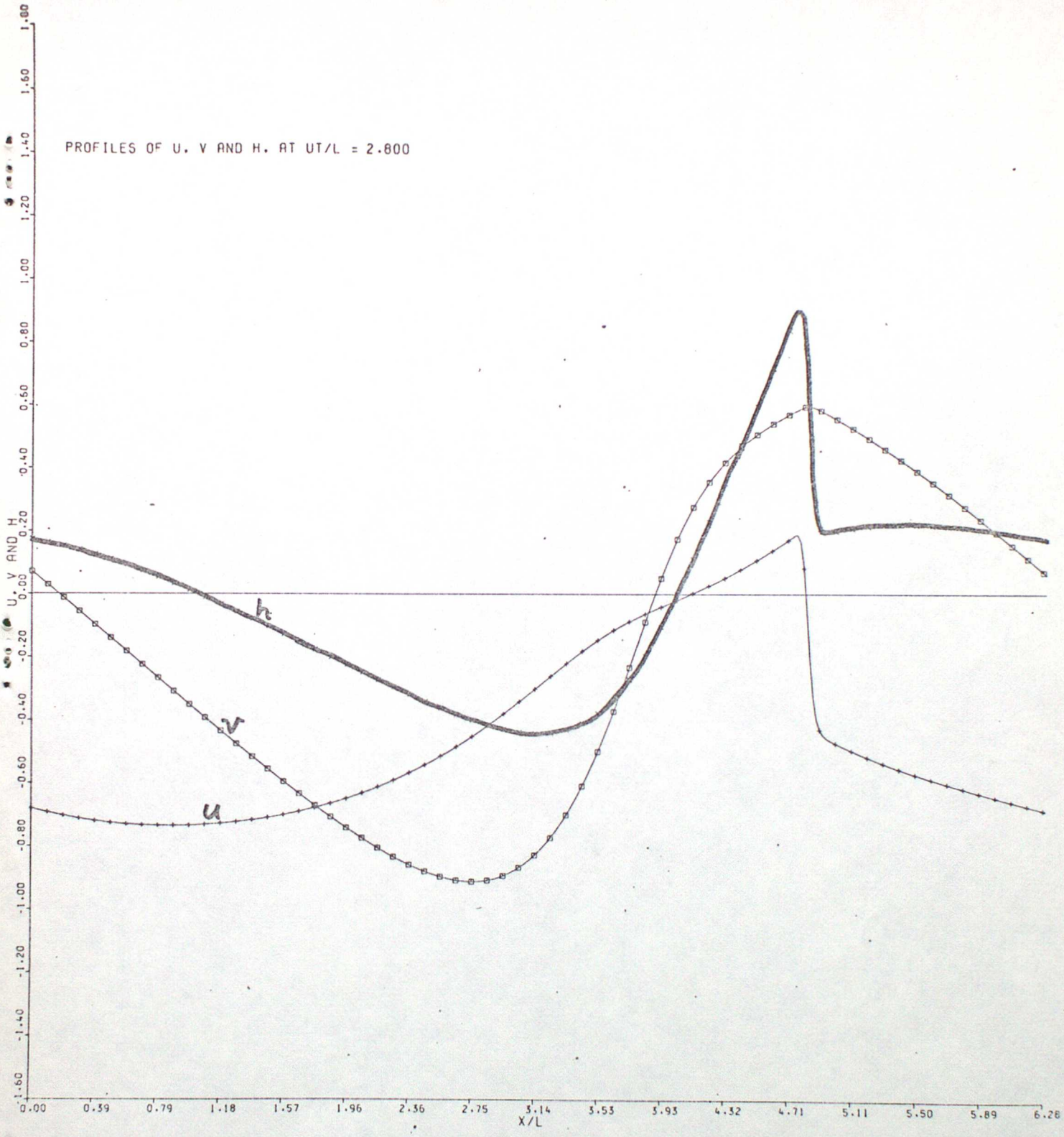

Figure 16. Results from F.D. model (b), at Ut/L = 2.8.

N = 320 and K = 2.5×10^{4} $m^{2}s^{-1}$.